

## Supporting Information

### Analysis of Sprout Spatial Distribution and Simulation

The 2D distances along the arc of the microcarriers were used as a proxy for the 3D distances. Fig. S1 shows the scatter plot of the 2D and 3D distances of pairs of sprouts (that are visible on the 2D projection) randomly placed on the surface of a microsphere.

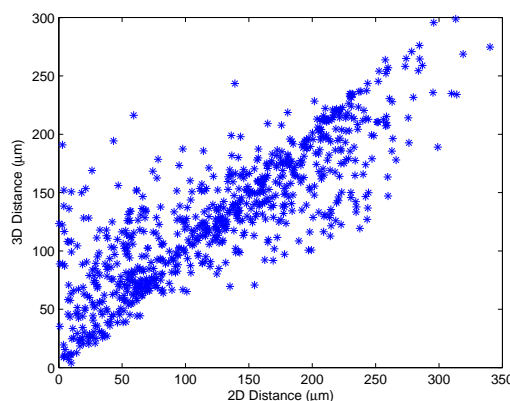


Figure S1: Scatter plot of 3D vs 2D distances of randomly placed sprouts. It can be seen that although there is not a one-to-one relationship, the 2D distances serve as a reasonable proxy for the 3D geodesic distances. The 3D geodesic distances were calculated with Vincenty’s formula for spheres.

In the simulation of Fig. 2d), the experimental size distribution of the microcarrier radius was collected (Fig. S2) as an estimate of pmf  $f_R(r)$  and was resampled during simulation to generate the radii  $r$ . While the variation in the radius of the microcarrier  $r$  appeared too small to affect the number of sprouts  $n_s$ , data was collected to ensure this independence (Fig. S3). The correlation between  $n_s$  and  $r$ ,  $n_s$  and  $r^2$ ,  $n_s$  and  $\ln(r)$  are respectively  $-0.067$ ,  $-0.064$ ,  $-0.072$ . These correlations are all insignificant, and in fact slightly negative, which further contradicts the notion that there may be more sprouts with greater surface area. Furthermore, regressions of  $n_s$  on  $r, r^2, \ln(r)$  also yield insignificant slopes. Thus,  $n_s$  does not seem to depend on  $r$  in this assay, and the marginal probability mass function  $f_{N_s}(n_s)$  can be used.

Similarly,  $n_s$  were generated by resampling the empirical distribution in Fig. 2a. Once  $n_s$  was drawn, the location  $(\theta, \phi)$  of each sprout was drawn from  $f_\Theta(\theta) = \frac{1}{2\pi}$  and  $f_\Phi(\phi) = \frac{1}{2} \sin \phi$ . The length of the sprout  $l$  was also resampled from the empirical data (Fig. S4). We chose to use the empirical distribution from the control experiment (The empirical distributions of  $n_s$  and  $l$  in both control and +DAPT gave almost identical simulation results). A sprout was determined to be visible if it protruded from the edge of the circle in the 2D maximum intensity projection, namely if  $(l + r) \sin \phi > r$ . The distance between each visible pair of the  $i^{th}$  and  $j^{th}$  sprouts was then computed:  $d_{i,j} = r(\min(|\theta_i - \theta_j|, 2\pi - |\theta_i - \theta_j|))$ . Note that the distribution of  $d_{i,j}$  generated from this simulation is different from merely  $r \cdot \theta$  where  $r$  is distributed as the experimental distribution and  $\theta$  distributed as  $\mathcal{U}[0, \pi)$ . This is because 1) the number of visible sprouts in a microcarrier

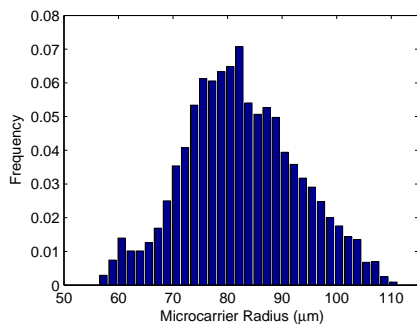


Figure S2: Histogram of radii of microcarriers, collected using a Hough transform algorithm on images of blank microcarriers ( $n > 2000$ ).

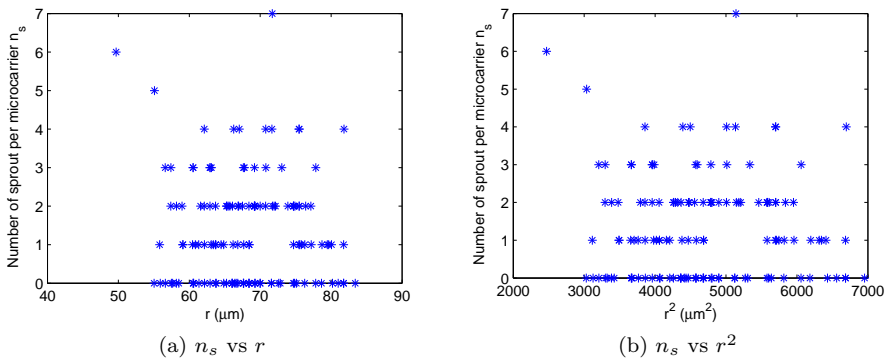


Figure S3: There appears to be no correlation between the number of sprouts  $n_s$  and radius of microcarrier  $r$ .

depends on the realization of  $r$ , and 2)  $d_{i,j}$  in the same microcarrier are dependent variables. They lead to the fact that the actual distribution of  $d_{i,j}$  depends intricately on the distribution of  $r$  and  $\theta$ .

### Sprout Detection Algorithm

Three-dimensional stacks of fluorescent images were loaded in Matlab. Images were first filtered with a 3D median filter with filter window size = 1 pixel. Each Z-slice was then further filtered with a 2D low pass filter with 1 pixel characteristic length scale of noise and 30 pixel characteristic object length. The first step in the measurement of sprout initiation was to identify the spherical microcarrier in each image. In the event when there were multiple microcarriers in view, the one closest to the center of the image was chosen. The radius  $r$  and center  $(x_c, y_c)$  of the microcarrier were determined using the generalized Hough transform to detect circles [1,2].

On a grayscale image, let the pixel intensity of pixel  $\mathbf{u}$  be  $s(\mathbf{u})$ . Edges of objects can be detected by computing the edge pixels  $\mathbf{u}_e$ , which are those pixels where the magnitude of the

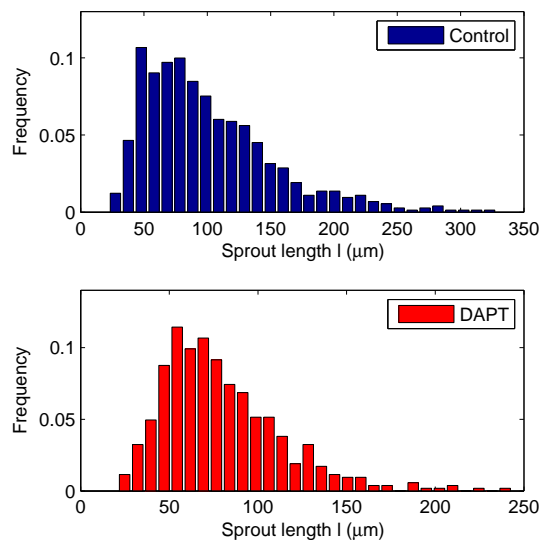


Figure S4: Histograms of sprout lengths ( $n > 500$  each).

gradients are greater than a threshold  $g$ . Namely,

$$\mathbf{u}_e \subseteq \mathbf{u} \ni \|\nabla s(\mathbf{u}_e)\| > g$$

Central to the method of Hough algorithm for analytic curves was the accumulation function  $A(\mathbf{a})$ . For a specific curve  $f(\mathbf{x}, \mathbf{a}) = 0$  with parameter vector  $\mathbf{a}$ ,  $A(\mathbf{a})$  was initialized to zero. Then for each  $\mathbf{u}_e$ , solve for all  $\mathbf{a}_s$  that satisfied the following equation:

$$f(\mathbf{u}_e, \mathbf{a}_s) = 0$$

In the special case of circle detection, this equation is equivalent to:

$$(x - x_0)^2 + (y - y_0)^2 - r_0^2 = 0$$

For each edge pixel  $\mathbf{u}_e$ , all the circles parameterized by  $\mathbf{a}_s = (x_0, y_0, r_0)$  containing  $u_e$  are incremented in the accumulator function:

$$A(\mathbf{a}_s) = A(\mathbf{a}_s) + 1$$

Note that in the algorithm,  $r_0$  was assumed to lie in a fixed range  $r_l \leq r_0 \leq r_u$ .  $\mathbf{a}_s$  was obtained by assuming a particular  $r_0$  in this range and solving for  $(x_0, y_0)$ . This is repeated for all other values of  $r_0$  in a fixed range. After each edge pixel  $\mathbf{u}_e$  is considered, the global maximum in  $A(\mathbf{a}_s)$  corresponds to the circle with radius  $r_0$  and center  $(x_0, y_0)$  with the most votes from all the edge pixels.

This algorithm was implemented in Matlab, and the pseudocode for choosing a center of a circle was:

```
HoughCircle() {
    FilterImage();
    ueAll=find(gradient>threshold);
    for ue in ueAll {
        for r0 in rRange{
            (x0,y0) = Solve(f(x,y,r)=0);
            A(r0,x0,y0) = A(r0,x0,y0)+1;
        }
    }
    [maxValue,ChosenCenter]=max(A(r0,x0,y0));
    return ChosenCenter;
}
```

This was done at each Z-plane (cyan circle on Fig. S5). On each Z-slice, two larger circles with radius  $r + 10$  and  $r + 45$  pixels was imposed around the center of the detected microcarrier (yellow and blue circles on Fig. S5). Any intensity protrusion within this ring was recorded. Fig. S5 illustrates the intensity protrusions on a particular Z-plane. By combining all the Z-slices, three-dimensional intensities were recorded around the microcarriers. In this three dimensional space, blocks of intensities that exceeded volume and intensity thresholds were counted as a sprout.

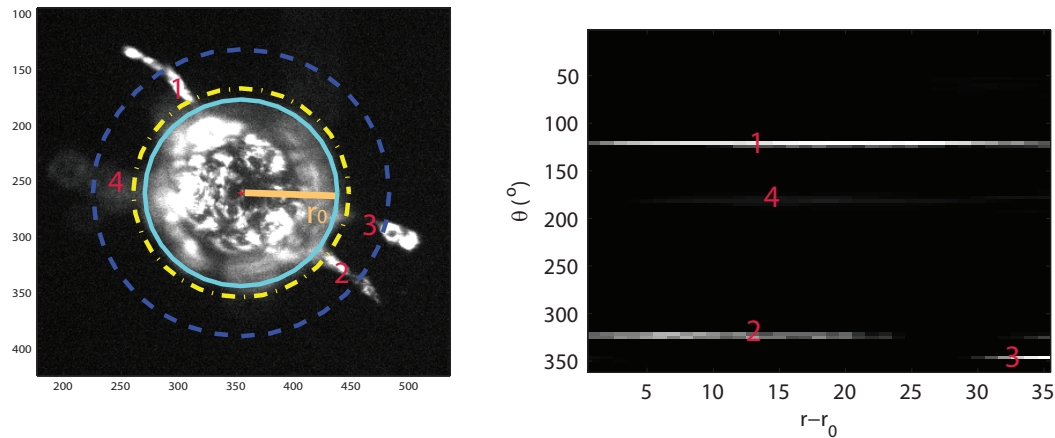


Figure S5: Demonstration of intensity protrusions on the  $(r, \theta)$  space. The intensities in the ring around the microcarrier (between the yellow circle and the blue circle) are plotted on the  $r - \theta$  space for a particular Z plane. The numbers denote the corresponding protrusions on the  $(x, y)$  space and  $(r, \theta)$  space. When sprout detection was done, blocks of intensities on the 3D  $(r, \theta, Z)$  space were identified.

## Statistical Inference of $r_a$

We want to test the significance of the intraclass correlation coefficient  $\rho$  against the following hypothesis of  $\rho = 0$ :

$$\begin{cases} H_0 : \rho = 0 \\ H_a : \rho \neq 0 \end{cases}$$

This can be done with a simple F test. The test statistic is the variance ratio, computed as  $F = \frac{MSA}{MSW}$ , which follows the F-distribution with degrees of freedom  $d_a = k - 1$  and  $d_w = N - k$ . The squared errors of the estimated intraclass correlation were approximated by [3]:

$$\hat{\sigma}^2 \simeq \frac{2(N-1)(1-r_a)^2[1+(u-1)r_a]^2}{u^2(N-k)(k-1)}$$

where

$$u = \frac{1}{k-1} \left( N - \frac{\sum n_i^2}{N} \right)$$

To test whether the  $\rho$ 's across conditions are equal, a two-sample  $Z$ -test was used [4,5].

## References

- [1] Tsuji, S. and Matsumoto, F. *IEEE Transactions on Computers* **C-27**(8), 777–781 August (1978).
- [2] Yuen, H., Illingworth, J., and Kittler, J. *Image and Vision Computing* **7**(1), 31–37 February (1989).
- [3] Swiger, L. A., Harvey, W. R., Everson, D. E., and Gregory, K. E. *Biometrics* **20**(4), 818–826 (1964).
- [4] Donner, A. and Wells, G. *Biometrics* **42**(2), 401–12 June (1986).
- [5] Young, D. J. and Bhandary, M. *Biometrics* **54**(4), 1363–73 December (1998).